PHYSICAL REVIEW B VOLUME 45, NUMBER 3 15 JANUARY 1992-I

Atomistic versus collective phenomena in catalysis: Carbidic and graphitic carbon on Ni(771)

R. Koch, O. Haase, M. Borbonus, and K. H. Rieder
Institut für Experimentalphysik, Freie Universität, Arnimallee 14, D-1000, Berlin 33, Germany
(Received 7 November 1991)

Carbidic and graphitic carbon overlayers on Ni(771) have been prepared, characterized by Auger electron spectroscopy, and investigated with scanning tunneling microscopy and low-energy electron diffraction. Ni(771)–a vicinal Ni(110) surface—proves an ideal model catalyst to disclose major differences between the two carbonaceous phases: The carbidic phase exhibits a (4×1) superstructure with isolated carbon atoms located at inner regions of the Ni(110) terraces. Graphitic carbon, on the other hand, forms a macromolecular surface arrangement that preferentially decorates and thus inactivates the catalytically active step sites.

The hydrogenation of carbon monoxide is an important step in the technological production of hydrocarbons from coal. Transition metals, like Fe, Ni, Co, Ru, and Rh,[1] are well known to act as catalysts in the Fischer-Tropsch synthesis of high-molecular-weight paraffinic compounds from CO. Among these metals, Ni selectively catalyses the formation of methane ($CO+3H_2=CH_4+H_2O$).[2] In previous studies of the kinetics of the CO hydrogenation on dispersed catalysts[3] as well as the dissociation of CO on single-crystal surfaces,[4–7] at least two different forms of surface carbon have been identified: (i) a carbidic phase, with unsaturated C $2p_z$ orbitals, that seems to be the active intermediate in the catalytic methane production, and (ii) a graphitic phase, that inactivates the catalyst (coking). Both phases are distinguished by the line shapes they exhibit in their Auger electron spectroscopy[5,6] (AES) and electron-energy-loss spectroscopy[7] (EELS) spectra.

In this paper we report scanning tunneling microscopy[8] (STM) results of carbidic and graphitic carbon on Ni(771), which represent real-space imaging of how the two carbon species affect the surface of a model catalyst. We chose Ni(771) for this study, a vicinal Ni(110) surface that in ideal bulk truncated form exhibits 1.23-nm-wide (110) terraces and steps parallel to the close-packed rows [see Fig. 1(a)]. On this model catalyst system, major differences between the two carbonaceous overlayers have been discovered: (i) The carbidic phase exhibits a (4×1) superstructure located at inner areas of the (110) terraces, near the ascent to the next terrace. (ii) The graphitic phase forms a chemically rather inert surface macromolecule, which preferentially decorates catalytically active step edges. Thus the STM images directly make visible how the active step sites of catalysts are inactivated when graphitic carbon is formed.

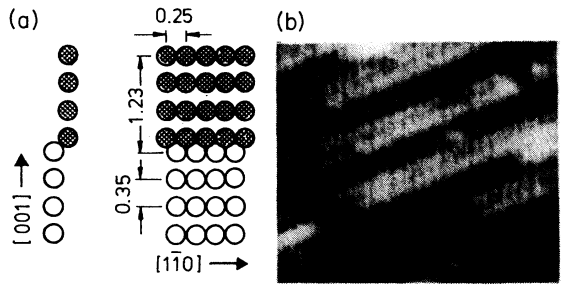

FIG. 1. (a) Sphere models of the side and top views of a fcc (771) surface (units in nm). (b) 6.5×5.7 nm^2 STM topview of clean Ni(771); to illustrate atomic resolution the linescan along the close-packed row marked with *B* is shown in Fig. 3(d); tunneling voltage $U_T=-24$ mV, tunneling current $I_T=10$ nA.

The experiments were performed in a UHV system that has been described in detail previously.[9] Besides the UHV scanning tunneling microscope the system is equipped with a four-grid retarding field analyzer for low-energy electron diffraction (LEED) and AES, a sputter gun, and facilities for heating and cooling the sample. The base pressure is better than 2×10^{-10} mbar. The sample was oriented by x-ray diffraction, cut by spark erosion and mechanically polished; it was further prepared in UHV by repeated cycles of Ne sputtering and heating to 1000 K until sharp LEED patterns were obtained. Figure 1(b) reproduces a topographical STM image of clean Ni(771) at atomic resolution without employing filtering techniques. In all the STM pictures presented here the steps ascend from bottom right to top left; for better utilization of the gray scale, however, the STM images have been tilted in such a manner that step edges appear to be at the same level. Figure 1(b) shows step configurations with in average three close-packed rows on each (110) terrace; the fourth row, which is part of the step to the next terrace [see Fig. 1(a), side view], is not resolved.[10] In Fig. 3(d) we present a line scan (*B*) along the direction marked in Fig. 1(b) to illustrate atomic resolution within the close-packed rows. The corrugation is about 0.01 nm in agreement with STM studies on flat metal surfaces.[11] The measured corrugation along [001] when crossing a step is 0.12 nm in agreement with crystal geometry. The carbidic overlayer was prepared by decomposition of CO at substrate temperatures of 550 K and CO partial pressures of 1×10^{-6} mbar; the carbidic phase can be transformed to the graphitic form by annealing at 700 K.

Figures 2(a) and 2(b) show AES spectra of the two carbon species detected on Ni(771). Figure 2(a) is obtained after CO dissociation at a substrate temperature of 550 K. The spectrum exhibits peaks at 251, 259, and 270

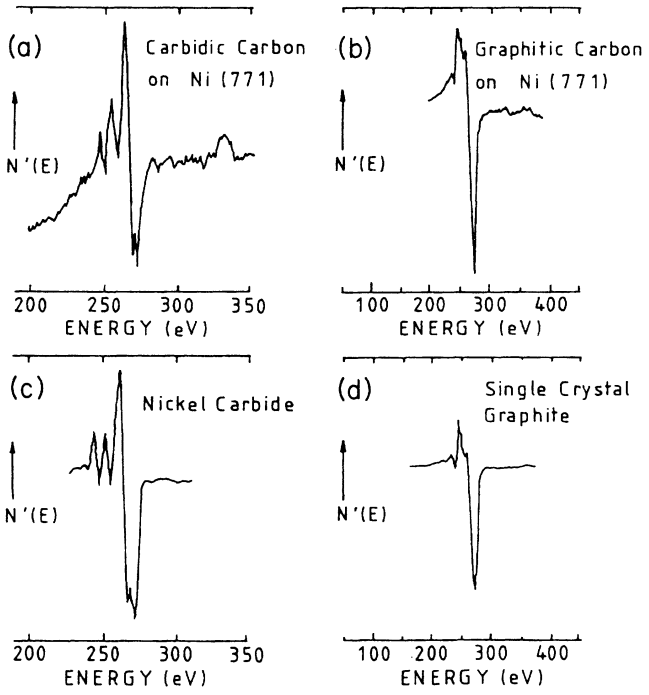

FIG. 2. AES spectra of (a) carbidic and (b) graphitic carbon on Ni(771) (primary energy $E_p = 2$ keV). AES spectra redrawn from Ref. 12 of (c) Ni_3C and (d) graphite.

eV as also found for carbon prepared under similar conditions on other Ni surfaces,[5] as well as on other Fischer-Tropsch metals.[6] Because of the similarity of the carbon AES line shape with that of Ni_3C [Fig. 2(c), redrawn from Ref. 12] this carbon phase has been termed "carbidic." Figure 2(b) displays the carbon AES spectrum after annealing the sample at temperatures above 700 K. It now exhibits one prominent peak at 270 eV and resembles the spectrum of pure graphite [Fig. 2(d), redrawn from Ref. 12]. In agreement with previous studies on Fischer-Tropsch metals,[5,6] we attribute this carbon species to the "graphitic" form. On Ni(771) the carbidic phase exhibits a (4×1) superstructure in the LEED pattern [Fig. 3(c)]. [Notice that our $(m \times n)$ notation refers to the lattice unit cell of the (110) terraces.] The intensity of the fractional LEED spots is comparable to the substrate spots even at small carbon coverages indicating a distortion of the Ni lattice. The appearance of the carbidic phase is accompanied by a sharpening of the reflections. The graphitic phase does not lead to additional spots in the LEED pattern with respect to the clean surface.

Figure 3(a) shows a topographic STM image of a Ni(771) surface region covered with carbidic carbon. According to the calibration of our piezoscanners, the average terrace width is 1.25 nm, which indicates the formation of predominantly single width terraces in accordance with LEED. On each terrace structures with a periodicity of 1.0 nm along $[1\bar{1}0]$ are detected in correspondence with the (4×1) in the LEED pattern. Compared with surface regions of clean Ni(771), where the regular step arrangement is frequently interrupted by kinks [see also Fig. 1(b)], uniform straight-lined step edges are formed over long distances in the carbon-covered regions. Carbidic carbon obviously stabilizes the formation of regular steps as confirmed by the sharpening of the LEED spots upon formation of the (4×1) superstructure. Figure 3(b) shows the carbidic phase at higher magnification together with carbon-free areas of the (110) terraces. To enhance contrast this image has been statistically differentiated.[13] The STM frequently resolves six protrusions on the (4×1) areas, three-by-three lying opposite each other [see marked circle and line scan *A* in Fig. 3(d)]. The vertical corrugation of these protrusions is approximately 0.02, 0.03, and 0.02 nm, respectively. The lower part of Fig. 3(b) contains clean parts of (110) terraces. These areas can be used to determine the position of the carbidic overlayer relative to the substrate lattice. Figure 3(b) definitely shows that the carbidic phase is located at the inner parts of the (110) terraces, near the ascent to the next terrace. *Notice that the step edges, which are commonly accepted to be active sites for chemical reactions,*[14] *are not covered by carbidic carbon.*

Figure 4(a) depicts a topographical STM image of a surface region covered with graphitic carbon. Compared with the carbidic phase the structure is completely different. The step configuration again is rather uniform, but now the periodicity along $[1\bar{1}0]$ is 0.25 nm, i.e., equal to that of the close-packed rows of the Ni(110) terraces in accordance with LEED. Club-shaped structures, ≈ 0.6 nm long, extend over the first two close-packed Ni rows starting at the step edges, as clearly seen in the line scan of Fig. 4(b); they frequently exhibit angles of $\approx 120°$ at their ends as found in the honeycomb configuration of graphite [see, e.g., the marked circle in Fig. 4(a)]. These structures are continued by 0.3-nm-long units, again often with hexagonal shapes. *As our central result we point to the fact that in contrast to carbidic carbon the graphitic phase occupies catalytically active step edges* [see the line scan of Fig. 4(b)], *making the well-known catalyst inactivation by coking directly visible.*

It is interesting to speculate on structural details for the two carbon overlayers on Ni(771) by referring to the bulk structures of Ni_3C and graphite, on the one hand, as suggested by AES, and the structural information provided by STM and LEED, on the other hand. In Ni_3C hexagonal layers of Ni and C atoms alternate with different azimuthal orientations, the two-dimensional (2D) Ni lattice being expanded by 6% compared with Ni(111); the carbon atoms in Ni_3C occupy threefold hollow sites of the Ni layers forming $(\sqrt{3}\times\sqrt{3})R30°$ superstructures as illustrated in Fig. 3(f). Assuming that the atomic configuration on the Ni(110) terraces is similar to the one in Ni_3C, the Ni lattice must undergo considerable local distortions under adsorption of carbidic carbon as signalled by the LEED intensities of the (1×4) superspots [appreciable distortions of the Ni substrate are also known to be induced by carbidic carbon on Ni(100) (Ref. 15)]. One plausible configuration which meets the requirement to account for the (1×4) periodicity observed with LEED and STM is shown in Fig. 3(e). A number of features observed in Fig. 3(b) [as indicated in the circle and line scan *A* of Fig. 3(d)] correspond to such a structure. The oc-

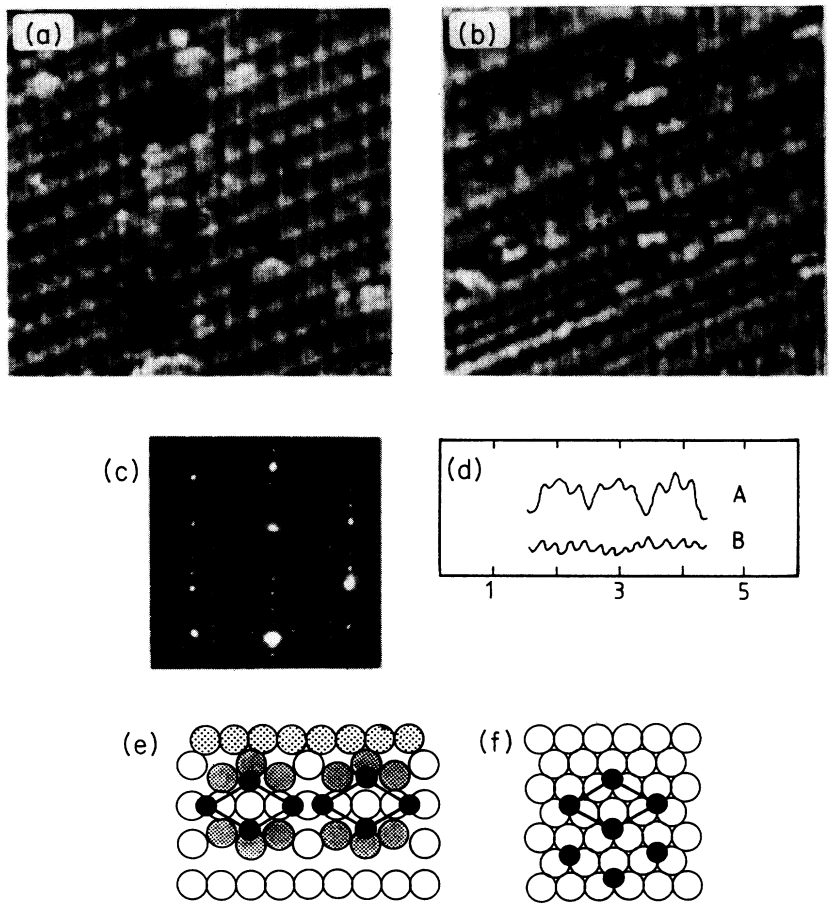

FIG. 3. (a) 15×14 nm^2 STM topview of the (4×1) superstructure of carbidic carbon on Ni(771). (b) Statistically differentiated 8.0×7.5 nm^2 STM topview of the carbidic phase together with carbon-free (110) terraces of Ni(771); $U_T = -100$ mV and $I_T = 10$ nA in both cases. Linescan along A is shown in (d); protrusions inside marked circle point to substrate distortions as modeled in (e). (c) (4×1) LEED pattern of Ni(771) covered with carbidic carbon ($E_p = 67$ eV). (d) Line-scans along marked directions in (b) (A) and Fig. 1(b) (B). Sphere models of the Ni-C configuration of (e) the "carbidic phase" on Ni(771) and (f) Ni_3C; black and grey circles represent carbon and distorted Ni atoms, respectively; the next terrace is indicated by dotted circles.

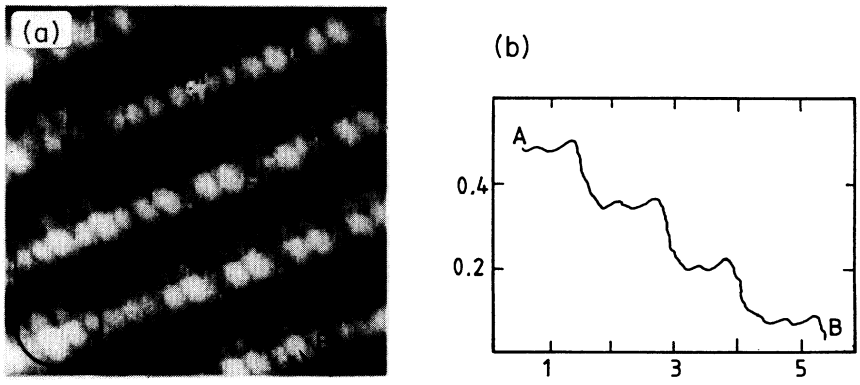

FIG. 4. (a) 4.8×5.0 nm^2 STM topview and (b) linescan [along $A \rightarrow B$ in (a)] of graphitic carbon on Ni(771) (units in nm); $U_T = -100$ mV, $I_T = 10$ nA. Notice that in contrast to carbidic carbon, Fig. 3(b), the graphitic carbon decorates the step edges and thus inactivates catalytically active adsorption sites.

currence of a diversity of other configurations in Fig. 3(b) may be due to locally varying carbon concentrations or to the well-known basic difficulty in imaging carbon overlayers.[16] Turning to the graphitic phase, we note that in bulk graphite the width of the honeycombs is 0.246 nm, which is only 1.2% smaller than the Ni-Ni distance along the close-packed rows. A linear chain of slightly stretched honeycombs in register with the Ni lattice along $[1\bar{1}0]$ therefore appears to be realistic. The distance between two honeycomb chains in graphite is 0.426 nm, which is about 20% larger than the lattice parameter of Ni(110) along [001] ($a_{Ni}=0.352$ nm). Due to the large mismatch between the two lattices along [001] a 2D graphitic overlayer coherent even over small distances cannot be expected to form on flat Ni(110).[17] At the step edges of Ni(771), with one end open for relaxation, a fragmentary honeycomb arrangement extending over two close-packed rows is observed [Fig. 4(a)]. Angles of 120° frequently observed with the STM at the step edges as well as on the terraces [see, e.g., marked circle in Fig. 4(a)] support this interpretation.

Summarizing our results, Ni(771) proved to be an ideal substrate to uncover major differences between the two carbonaceous phases: Carbidic carbon was found to yield (4×1) LEED patterns; by simultaneously imaging overlayer and substrate regions, STM revealed that the (4×1) structural elements are located at inner areas of the (110) terraces, near the ascent to the next terrace. The graphitic phase, on the other hand, preferentially decorates catalytically active step sites and thus reduces the activity and possibly the selectivity of catalysts. Regarding structural aspects we combined our STM, LEED, and AES results with data on bulk Ni_3C and graphite to propose plausible models for the surface structures of the two carbonaceous species: In the carbidic phase the carbon atoms very likely distort the Ni lattice to form a structure similar to that of Ni_3C. The nearest-neighbor distance of the carbon atoms then is about 0.45 nm, which is about 3 times the C-C bond length in organic compounds (0.12–0.15 nm). This means that there is only weak bonding between the carbidic carbons, thus explaining their chemical reactivity against coadsorbates like hydrogen[3] or water.[18] The carbon atoms of the graphitic phase, on the other hand, seem to exhibit a structure similar to the one found in graphite (C-C bond length is 0.142 nm), pointing to strong in-plane bonding. Consequently, in addition to decorating the active step sites, the graphitic phase affects the catalytic activity of the metal in another way: Its electronic properties are similar to those of organic macromolecules, which, in general, are inert against chemical attacks.

The authors wish to thank Christian Roth for technical assistance and acknowledge financial support by the Deutsche Forschungsgemeinschaft (Sfb 6).

[1]M. A. Vannice, Catal. Rev. **14**, 153 (1976); J. Catal. **37**, 449 (1975); M. Boudart and M. A. Mc Donald, J. Chem. Phys. **88**, 2185 (1984).

[2]M. A. Vannice, J. Catal. **44**, 152 (1976).

[3]J. A. Rabo, A. P. Risch, and M. L. Poutsma, J. Catal. **53**, 295 (1978); M. Araki and V. Ponec, *ibid.* **44**, 439 (1976).

[4]H. H. Madden and G. Ertl, Surf. Sci. **35**, 211 (1973); P. K. Wang, J. P. Ansermet, Ch. P. Slichter, and J. H. Sinfelt, Phys. Rev. Lett. **55**, 2731 (1985); T. M. Duncan, P. Winslow, and A. T. Bell, Chem. Phys. Lett. **102**, 163 (1983).

[5]D. W. Goodman, R. D. Kelley, T. E. Madey, and J. T. Yates, J. Catal. **63**, 226 (1980); R. Rosei, F. Ciccacci, R. Memeo, C. Mariani, L. S. Caputi, and L. Papagno, J. Catal. **83**, 19 (1983).

[6]J. E. Houston, D. E. Peebles, and D. W. Goodman, J. Vac. Sci. Technol. A **1**, 995 (1983); D. W. Goodman and J. M. White, Surf. Sci. **90**, 201 (1979); H. P. Bonzel and H. J. Krebs, *ibid.* **91**, 499 (1980).

[7]L. Papagno, L. S. Caputi, F. Ciccacci, and C. Mariani, Surf. Sci. **128**, L209 (1983); L. S. Caputi, G. Chiarello, and L. Papagno, *ibid.* **162**, 259 (1985).

[8]G. Binnig and H. Rohrer, Rev. Mod. Phys. **59**, 615 (1987).

[9]O. Haase, M. Borbonus, R. Koch, and K. H. Rieder, Rev. Sci. Instrum. **61**, 1480 (1990).

[10]O. Haase, R. Koch, M. Borbonus, and K. H. Rieder, Phys. Rev. Lett. **66**, 1725 (1991).

[11]F. Jensen, F. Besenbacher, E. Laesgaard, and I. Stensgaard, Phys. Rev. B **42**, 9206 (1990).

[12]C. C. Chang, in *Analytical Auger Electron Spectroscopy. Characterization of Solid Surfaces,* edited by P. F. Kane and G. B. Larrabee (Plenum, New York, 1974).

[13]R. J. Wilson and S. Chiang, J. Vac. Sci. Technol. A **6**, 398 (1988).

[14]R. J. Gale, M. Salmeron, and G. A. Somorjai, Phys. Rev. Lett. **38**, 1027 (1977); L. K. Verheij, M. B. Hugenschmidt, L. Cölln, B. Poelsema, and G. Comsa, Chem. Phys. Lett. **166**, 523 (1990).

[15]J. H. Onuferko, D. P. Woodruff, and B. W. Holland, Surf. Sci. **87**, 357 (1979); M. Bader, C. Ocal, B. Hillert, J. Haase, and A. M. Bradshaw, Phys. Rev. B **35**, 5900 (1987).

[16]G. K. Binnig, H. Rohrer, Ch. Gerber, and E. Stoll, Surf. Sci. **144**, 321 (1984).

[17]L. Papagno and L. S. Caputi, Phys. Rev. B **29**, 1483 (1984).

[18]J. A. Rabo, J. N. Francis, and L. F. Elek, in Proceedings of the Catalysis Congress, Tokyo, 1980 (unpublished).

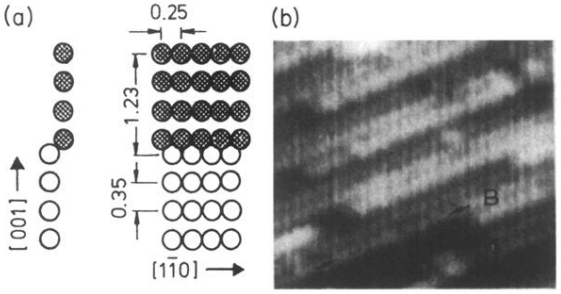

FIG. 1. (a) Sphere models of the side and top views of a fcc (771) surface (units in nm). (b) 6.5×5.7 nm^2 STM topview of clean Ni(771); to illustrate atomic resolution the linescan along the close-packed row marked with *B* is shown in Fig. 3(d); tunneling voltage $U_T = -24$ mV, tunneling current $I_T = 10$ nA.

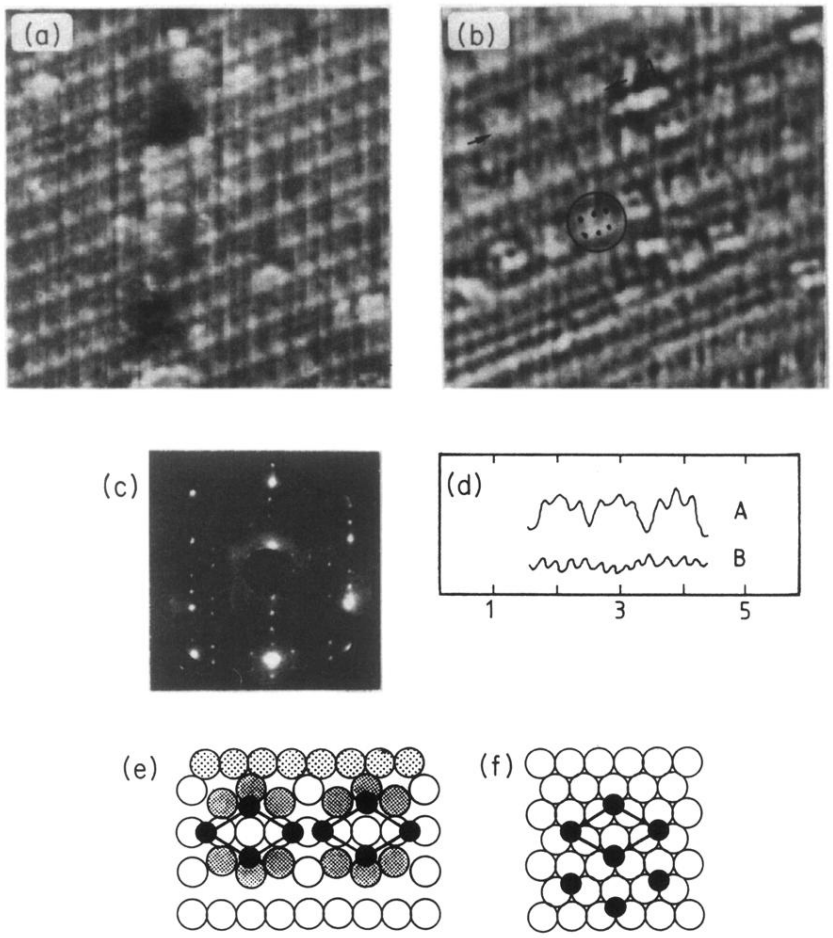

FIG. 3. (a) 15×14 nm^2 STM topview of the (4×1) superstructure of carbidic carbon on Ni(771). (b) Statistically differentiated 8.0×7.5 nm^2 STM topview of the carbidic phase together with carbon-free (110) terraces of Ni(771); $U_T = -100$ mV and $I_T = 10$ nA in both cases. Linescan along A is shown in (d); protrusions inside marked circle point to substrate distortions as modeled in (e). (c) (4×1) LEED pattern of Ni(771) covered with carbidic carbon ($E_p = 67$ eV). (d) Line-scans along marked directions in (b) (A) and Fig. 1(b) (B). Sphere models of the Ni-C configuration of (e) the "carbidic phase" on Ni(771) and (f) Ni_3C; black and grey circles represent carbon and distorted Ni atoms, respectively; the next terrace is indicated by dotted circles.

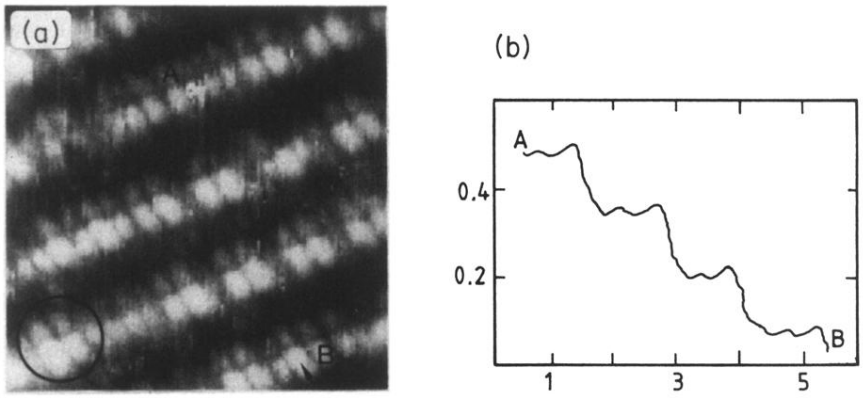

FIG. 4. (a) 4.8×5.0 nm^2 STM topview and (b) linescan [along $A \rightarrow B$ in (a)] of graphitic carbon on Ni(771) (units in nm); $U_T = -100$ mV, $I_T = 10$ nA. Notice that in contrast to carbidic carbon, Fig. 3(b), the graphitic carbon decorates the step edges and thus inactivates catalytically active adsorption sites.